J. Fluid Mech. (1968), *vol.* 33, *part* 2, *pp.* 337–351
Printed in Great Britain

Hydromagnetic surface waves with alternating magnetic fields

By MICHAEL J. SCHAFFER

Department of Electrical Engineering, Massachusetts Institute of Technology, Cambridge, Massachusetts†

(Received 20 October 1967)

Hydromagnetic surface waves propagating on the surface of a finitely conducting fluid are studied experimentally and theoretically. An alternating magnetic field is used, so that the field is largely excluded from the bulk of the fluid. Thus, the magnetic damping of the waves is negligible, and the perfectly conducting d.c. case is simulated. The effects of a finite electromagnetic skin depth, δ, are included in the calculation of the theoretical wave dispersion relation. It is predicted that as δ is increased and becomes comparable to the wavelength of the surface wave, the effect of the magnetic field on the fluid motion is decreased. This prediction is confirmed experimentally.

1. Introduction

The conductivity of available liquid metals is so low that laboratory observation of hydrodynamic surface waves with a d.c. applied magnetic field of the type discussed by Rook (1964) is very difficult. Electromagnetic damping of the wave motion is the dominant effect. However, if a high frequency alternating magnetic field with a small skin depth is applied above a conducting fluid, the magnetic field is excluded from the bulk of the fluid, and hydromagnetic surface waves can be observed. This paper describes the experimental observation of plane hydromagnetic waves similar to those shown in figure 1, and compares the experiment with a theoretical analysis which includes the effects of a finite skin depth.

The applied magnetic field, $H_p \cos \omega_m t$, is parallel to the direction in which the waves propagate on the surface of the fluid (the z-direction in figure 1). Because the magnetic field is excluded from the fluid, the magnetic field lines must follow the wave contour of the interface. It is apparent from the figure that the magnitude of the magnetic field is greater at the peaks of the wave than at the valleys. Therefore, the magnetic field exerts a greater pressure at the peaks than at the valleys, producing a magnetic restoring force.

Waves of this sort were first treated analytically by Kruskal & Schwarzchild (1954) for a perfectly conducting fluid with a d.c. magnetic field. A later analysis (Melcher 1963) included the effects of surface tension, as well as the effects of bounding walls at $x = b$ and $x = -a$. This analysis, too, was based on a perfectly

† Present address: Department of Physics, Escuela de Ingenieros Industriales, Universidad Tecnica del Estado, Santiago, Chile.

conducting fluid model. The dispersion relation relating the frequency of the surface wave to its wave number, $k = 2\pi/\lambda$, obtained by Melcher, is

$$\omega^2\rho \coth(ka) = Tk^3 + \rho gk + \mu_0 H_0^2 k^2 \coth(kb), \tag{1}$$

where

$\omega = 2\pi f$ = frequency of the surface wave,

ρ = mass density of the fluid,

T = surface tension of the fluid,

g = acceleration of gravity, taken as a positive number of the system of figure 1,

H_0 = unperturbed d.c. magnetic field in amperes/meter (rationalized MKS units),

μ_0 = magnetic permeability of free space.

a, b are defined in figure 1.

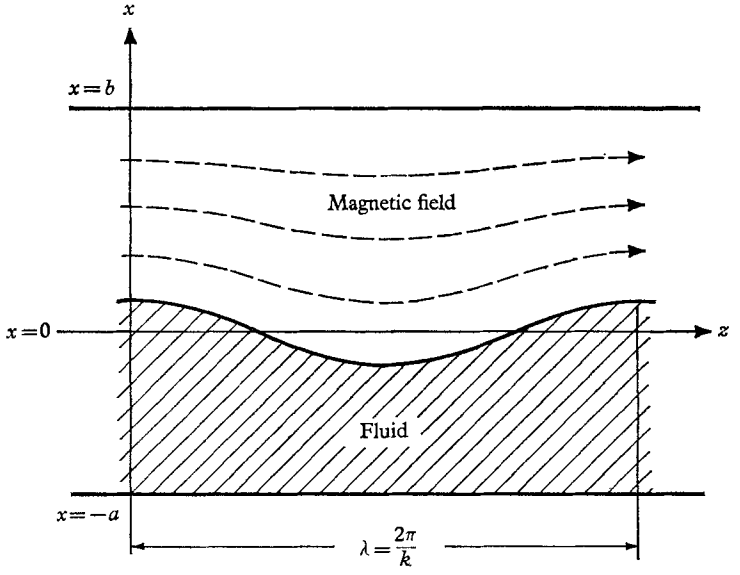

FIGURE 1. Hydrodynamic surface waves with the magnetic field excluded from the fluid.

Generalization of Melcher's theory is achieved by substituting the r.m.s. a.c. magnetic field strength $H_p/\sqrt{2}$ for the d.c. field strength, H_0. This substitution is justified by the experiments of Colgate, Furth & Halliday (1960), in which the equilibrium of liquid sodium metal in the presence of an alternating magnetic field agreed closely with predictions based on the use of the r.m.s. field strength. Further justification is given by the experiments of Devitt & Melcher (1965) in which quantitative agreement is obtained for electrohydrodynamic waves between a theory based on a d.c. electric field and an experiment using an a.c. electric field. This simple extension of the d.c. theory will not be valid, however when the magnetic skin depth δ exceeds approximately one-tenth of the length of the surface wave.

Alternating field hydromagnetics already has practical application: the melting and processing of metals while levitated in an alternating magnetic

field (Chandrasekhar 1961; Okress, Wroughton, Comentz, Brace & Kelly 1952 Peifer 1965; Zhezherin 1959). It has frequently been noted that the maximum amount of molten metal which can be levitated stably depends on the surface tension of the liquid being levitated (Okress *et al.* 1952; Zhezherin 1959; Weisberg 1959). For larger quantities of metal, the liquid metal is observed to drip or run from the bottom of the suspended fluid, where there is usually a null in the magnetic field. Such instability severely limits the amount of fluid that can be levitated at any one time. Zhezherin has suggested the use of auxiliary magnetic fields at frequencies different from that of the main levitation field to stabilize the surface of the fluid in the null region. Intelligent design of such a stabilized system must include a dynamic stability analysis in terms of hydromagnetic surface waves.

In another field, Osovets (1963) has reviewed the numerous proposals that have been advanced for enhancing the stability of plasma containment systems through the use of alternating magnetic fields, either alone or in conjunction with a steady magnetic field.

2. Observation of hydromagnetic surface waves in NaK

Experiments performed to observe hydromagnetic surface waves in alternating magnetic fields involved values of δk from 0·05 up to 0·65. Eutectic NaK (22 % sodium, 78 % potassium) in an evacuated system was used as the conducting fluid.

Description of the experiment

The surface waves were excited in a glass-covered, rectangular container or resonator, which was constructed from annealed, oxygen-free copper. The resonator chamber was evacuated to a pressure of about 10^{-3} torr prior to filling with

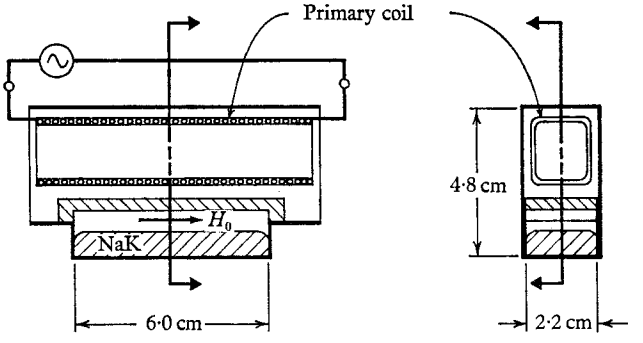

FIGURE 2. Essential features of the experimental surface wave fluid resonator.

NaK, in order to limit the amount of oxide which formed on the surface of the NaK. Other basic features of the resonator and the means for generating the alternating magnetic field are shown schematically in figure 2. The resonator was filled to a depth of 0·6 to 1·0 cm with NaK. The side walls of the resonator extended upward 4·8 cm from the bottom and were joined at the top by a copper piece, to provide a closed path for the alternating currents which flowed across the surface of the fluid and generated the magnetic field. A long solenoidal coil coupled

the resonator system to either a 6 kc/s alternator or a 130 kc/s vacuum tube power generator. The resonator and the coil were cooled by forced circulation of kerosene. The unperturbed magnetic field above the fluid was measured by the voltage induced in a small probe coil inserted in the region between the glass cover and the solenoid. Relative motion of the fluid was detected by the fluctuations in the amplitude of the magnetic field. Surface waves were excited in the resonator either by shaking the whole resonator mechanically, or by perturbing the magnetic field at one end of the resonator.

The shaking frequencies which produced the largest relative fluid motion, as determined by the magnetic field fluctuations, were recorded as the resonance frequencies. The resonances that correspond to zero magnetic field were actually observed with a small magnetic field applied. This field was large enough so that the fluid motion could be observed with the probe, but it was far too small to produce any significant force in the system.

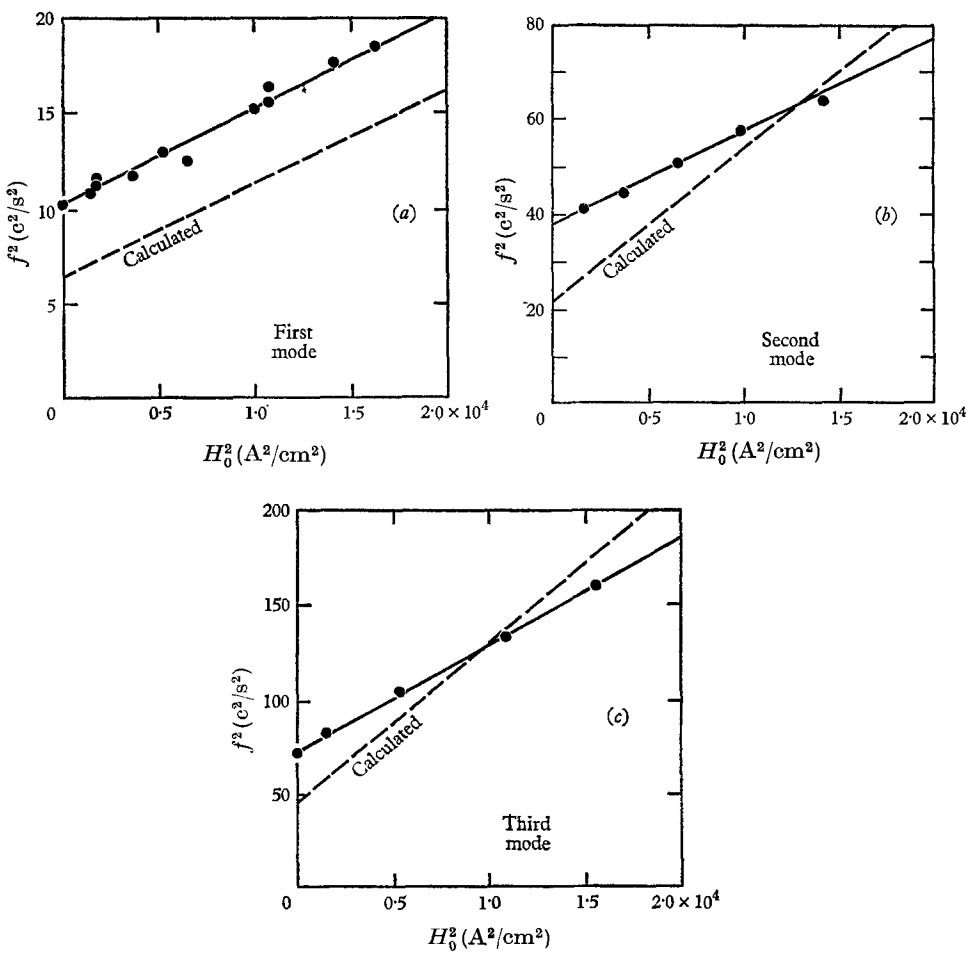

FIGURE 3. Experimental results of frequency *vs.* magnetic field for: (*a*) first mode ($\lambda \approx 12$ cm); (*b*) second mode ($\lambda \approx 6$ cm); and (*c*) third mode ($\lambda \approx 4$ cm), using a 130 kc/s magnetic field. Dotted lines indicate the curves calculated from d.c. theory.

Experimental results

The square of the observed resonance frequencies for the first, second, and third modes is plotted against the mean square magnetic field, $H_0^2 = \frac{1}{2}H_p^2$ in figure 3. The experimental points fall very nearly on a straight line, thus verifying the functional dependence of the frequency shift on the applied magnetic field that was predicted by the dispersion relation (1). The experimentally observed

	Calculated		Observed	
Mode	f(c/s) for $H_0 = 0$	$\frac{f^2}{H_0^2}\left(\frac{c^2/s^2}{A^2/cm^2}\right)$	f(c/s) for $H_0 = 0$	$\frac{f^2}{H_0^2}\left(\frac{c^2/s^2}{A^2/cm^2}\right)$
1	2·54	$5{\cdot}0 \times 10^{-4}$	3·25	$5{\cdot}0 \times 10^{-4}$
2	4·8	$3{\cdot}2 \times 10^{-3}$	6·2	$1{\cdot}9 \times 10^{-3}$
3	6·85	$8{\cdot}3 \times 10^{-3}$	8·6	$5{\cdot}7 \times 10^{-3}$

TABLE 1

resonance frequencies with no magnetic field applied and the observed values of the slope $\Delta f^2/\Delta H_0^2$ are compared in table 1 to the corresponding quantities calculated from (1). The calculations are made on the basis of $a = 1{\cdot}0$ cm; $b = 3{\cdot}8$ cm, the distance between the free surface and the top plate; and that the wavelengths for the first, second and third modes are 12·0 cm, 6·0 cm and 4·0 cm respectively.

The discrepancy between the calculated and the observed values for the zero-field resonance frequencies is due to the highly idealized assumption that the modes in the resonator are simply multiple half-wave segments of an infinite train of plane waves. In actual fact, the free surface of the NaK is observed to stick to the walls of the resonator at some places, and to slide more or less freely at others. Moreover, this pattern of sliding and sticking can change from day to day. Sticking lowers the wavelengths of the natural modes by an amount that depends on the surface tension of the fluid, thereby raising the natural frequencies of the resonator. It is not surprising, then, that the observed natural frequencies in the resonator are some 30 % higher than the values listed in the first column of the table.

There is also a sizeable discrepancy between the observed and the calculated values of the frequency shift slope $\Delta f^2/\Delta H_0^2$, for the second and third modes. Actually, the experimental frequency shift is observed to vary from day to day, presumably because the variations in the pattern of sticking and sliding at the walls give rise to changes in the natural mode configurations.

Thus, the k entering into equation (1) is not simply 2π divided by a submultiple of 12 cm, but an effective value corresponding to the complex of modes that actually exist in the system. Furthermore, (1) does not account for fringing of either the applied magnetic field or its perturbed components at the open ends of the resonator system.

However, in spite of the discrepancies, it is apparent that hydromagnetic surface waves are observed, and that their properties are essentially as predicted.

To determine the effect of changing the electromagnetic skin depth, frequency shift *vs.* magnetic field strength data was taken at two different magnetic field frequencies, 6·0 and 130 kc/s, corresponding to skin depths of about

$$4{\cdot}15 \times 10^{-3}\,\mathrm{m} \quad \text{and} \quad 0{\cdot}895 \times 10^{-3}\,\mathrm{m}$$

respectively. The results for the third mode waves, corresponding to δk of about 0·63 and 0·14 at the two field frequencies respectively, are plotted in figure 4*a*.

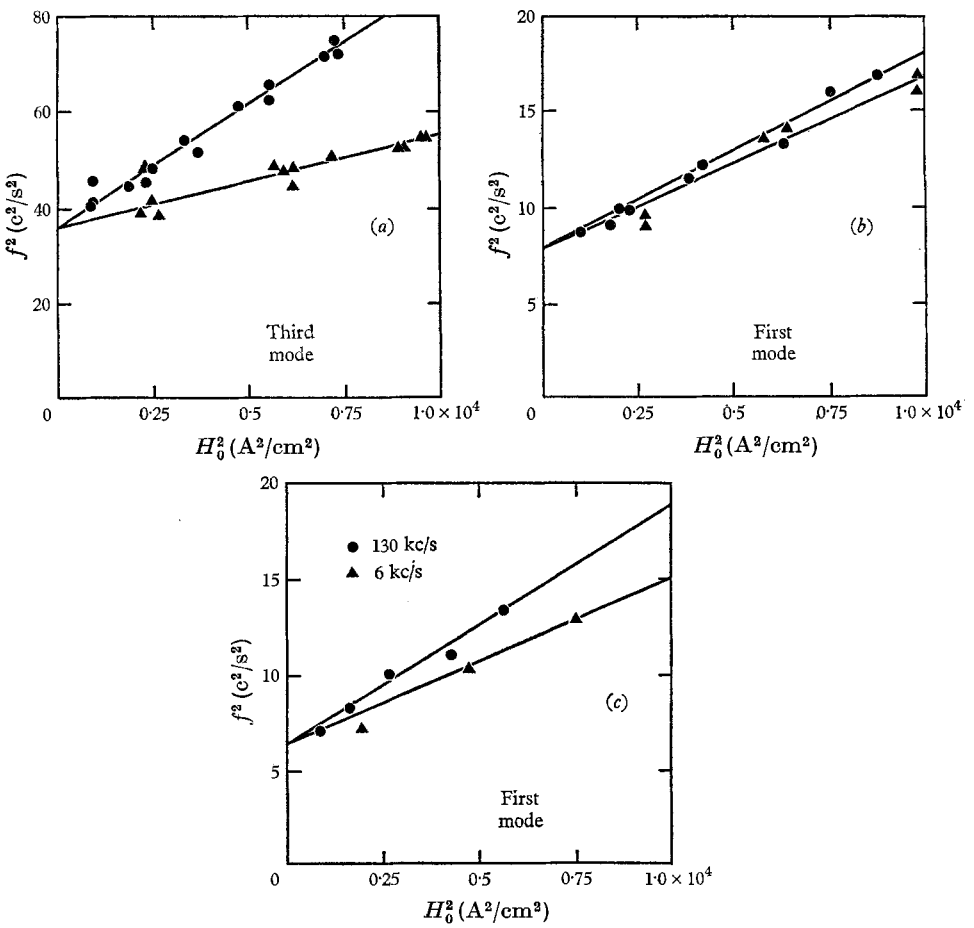

FIGURE 4. Experimental results of frequency *vs.* magnetic field for two different skin depths: (*a*) third mode, (*b*) first mode; (*c*) first mode, same system, but 16 days later.

The frequency shift slope at the larger skin depth is less than half the slope at the smaller skin depth. The results for the first mode waves, corresponding to δk values of about 0·21 and 0·046 respectively for the two frequencies, are plotted in figure 4*b*, *c*. The difference between the frequency shifts at the two different skin depths is not so large as with the third mode, but it is still significant.

In both cases, the lower frequency field is less effective in shifting the resonance frequencies of natural wave modes in the resonator than the higher frequency field, since in the large skin depth case the field does not interact as strongly with

the fluid wave. As the skin depth increases and becomes comparable to the wavelength of the surface wave, the surface waves produce less and less distortion of the applied magnetic field. As is shown qualitatively in figure 5, the magnetic field begins to penetrate the surface perturbations almost as if they were not there. A quantitative theory of hydromagnetic surface waves is now developed for the case of small, but non-zero, skin depths.

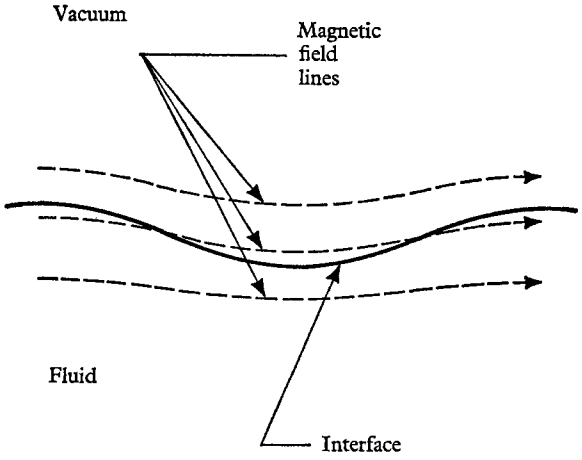

FIGURE 5. Appearance of the magnetic field near the surface of a conducting fluid with a sinusoidal surface perturbation.

3. Finite skin depth analysis

The generalization of the wave dispersion relation (1) for finite skin depth penetration, is obtained by solving for the wave motion of the fluid under the influence of forces due to a magnetic field which penetrates the fluid. The linearized equation of motion and the equation of continuity for an incompressible fluid without viscosity are

$$\rho \frac{\partial^2 \boldsymbol{\xi}}{\partial t^2} = -\nabla p + \nabla \cdot \mathbf{M} \tag{2}$$

and

$$\nabla \cdot \boldsymbol{\xi} = 0, \tag{3}$$

where $\boldsymbol{\xi}$ is the vector displacement of the fluid, p is the fluid pressure, and $\nabla \cdot \mathbf{M}$ gives the magnetic force density in the fluid. When the applied magnetic field is uniform above the fluid and applied in the z-direction, as in figure 1, and if the surface waves are propagating in the z-direction, the linearized Maxwell stress tensor can be written as

$$\mathbf{M} = \mu_0 \begin{bmatrix} -(\frac{1}{2}H_{0z}^2 + H_{0z}h_{fz}) & H_{0z}h_{fx} \\ H_{0z}h_{fx} & (\frac{1}{2}H_{0z}^2 + H_{0z}h_{fz}) \end{bmatrix}, \tag{4}$$

where

$$H_{0z} = H_p e^{x/\delta} \cos(\omega_0 t + x/\delta) \tag{5}$$

is the magnetic field arising from ordinary skin depth penetration of a conductor at a plane surface, and h_{fx} and h_{fz} are the x- and z-components of the small perturbations to this magnetic field due to the waves in the fluid. In writing equation (5) for H_{0z} it is assumed that $a \gg \delta$, so that the effect of the bottom of the fluid on the magnetic field can be neglected. The equations for the magnetic

field in an ohmically conducting fluid, when the electric displacement current is negligible, are

$$\frac{\partial \mathbf{H}}{\partial t} - \frac{1}{\mu_0 \sigma} \nabla^2 \mathbf{H} = \nabla \times \left(\frac{\partial \boldsymbol{\xi}}{\partial t} \times \mathbf{H} \right) \tag{6}$$

and

$$\nabla \cdot \mathbf{H} = 0, \tag{7}$$

where σ is the electrical conductivity of the fluid.

Equations (2) to (7) must be solved simultaneously if an exact linearized solution is to be obtained. A considerable simplification results, however, if the response of the fluid to the high frequency components of the magnetic force density is neglected. Since the ratio of the fluid wave frequency to the magnetic field frequency, ω/ω_0, is less than 0·002 in all the experiments performed, this simplification is well founded. A further simplification is obtained if the motional term $\nabla \times \{(\partial \boldsymbol{\xi}/\partial t) \times \mathbf{H}\}$ in equation (6) for the magnetic field is dropped. Neglecting this term affects the magnetic field calculated from (6) and (7) only at order ω/ω_0 and higher. These motional effects on the magnetic field would be important in the calculation of electrical damping or of parametric interaction of the field with the fluid; but they are not necessary for deriving a dispersion relation which explains the experimental results presented in figure 4. With this simplification, the magnetic field can be calculated independently of the fluid motion, except for the condition that the field be continuous at the perturbed fluid interface.

Magnetic field and force density

In order to satisfy the condition of magnetic field continuity at the perturbed interface, the components h_{fx} and h_{fz} of the perturbed magnetic field in the fluid must be of the same period in z and must contain the sum-and-difference frequencies $\omega_\pm = \omega_0 \pm \omega$. A suitable solution for this magnetic field when $a \gg \delta$, which can be verified by substitution into (6) and (7) is

$$h_{fx} = \sum_{\pm} e^{\alpha x} \sin(kz) \left[h_{f1} \cos(\omega_\pm t + \beta x) + h_{f2} \sin(\omega_\pm t + \beta x) \right], \tag{8}$$

$$h_{fz} = \sum_{\pm} e^{\alpha x} \cos(kz) \left[h_{f1} \left\{ \frac{\alpha}{k} \cos(\omega_\pm t + \beta x) - \frac{\beta}{k} \sin(\omega_\pm t + \beta x) \right\} + h_{f2} \left\{ \frac{\beta}{k} \cos(\omega_\pm t + \beta x) + \frac{\alpha}{k} \sin(\omega_\pm t + \beta x) \right\} \right]. \tag{9}$$

Neglecting factors of order ω/ω_0, the space-rate constants α and β must satisfy the conditions

$$\alpha^2 - \beta^2 = k^2, \tag{10}$$

$$\alpha\beta = \tfrac{1}{2}\omega_0 \mu_0 \sigma = 1/\delta^2. \tag{11}$$

The coefficients h_{f1} and h_{f2} are to be determined by the requirement of field continuity at the fluid interface, $x = \xi_0 \cos(kz) \cos(\omega t)$. The details of matching this boundary condition and calculating the two field coefficients are contained in the appendix.

Using the magnetic field quantities given in (5), (8) and (9), the Maxwell stress tensor can be computed from (4). Expanding trigonometric products of the

form $[\cos(\omega_\pm t+\beta x)\cos(\omega_0 t+x/\delta)]$ into a sum of the component frequency terms, and dropping the high frequency component terms, the wave frequency magnetic force density in the fluid is

$$\begin{aligned}\nabla\cdot\mathbf{M} = \frac{\mu_0 H_p}{\delta}\exp\{(\alpha+1/\delta)x\}\cos\omega t \\ \times\Big[\mathbf{i}_x\Big\{-\Big(\frac{2}{\delta k}h_{f2}+\frac{\alpha+\beta}{k}h_{f1}+\frac{\beta-\alpha}{k}h_{f2}\Big)\cos\Big(\beta-\frac{1}{\delta}\Big)x \\ +\Big(\frac{2}{\delta k}h_{f1}+\frac{\beta-\alpha}{k}h_{f1}-\frac{\alpha+\beta}{k}h_{f2}\Big)\sin\Big(\beta-\frac{1}{\delta}\Big)x\Big\}\cos kz \\ +\mathbf{i}_z\{(h_{f1}-h_{f2})\cos\{\beta-(1/\delta)\}x \\ +(h_{f1}+h_{f2})\sin\{\beta-(1/\delta)\}x\}\sin kz\Big],\end{aligned} \tag{12}$$

where the steady pressure due to the $\frac{1}{2}\mu_0 H_{0z}^2$ term in (4) has also been dropped.

Fluid motion and pressure

The fluid motion is now obtained from (2) and (3), using (12). The fluid displacement vector $\boldsymbol{\xi}$ is separated into a curl-free component and a component with curl

$$\boldsymbol{\xi} = \boldsymbol{\xi}_1+\boldsymbol{\xi}_2, \tag{13}$$

where $$\nabla\times\boldsymbol{\xi}_1 = 0 \quad\text{and}\quad \nabla\times\boldsymbol{\xi}_2 \neq 0. \tag{14), (15}$$

Since an additional curl-free component with non-zero divergence can always be added to $\boldsymbol{\xi}_1$ and subtracted from $\boldsymbol{\xi}_2$ without destroying the separation defined by (13) to (15), it is convenient to require that $\boldsymbol{\xi}_1$ and $\boldsymbol{\xi}_2$ satisfy (3) individually. Then, taking the curl of (2) twice in succession, the following set of equations is obtained for $\boldsymbol{\xi}_1$ and $\boldsymbol{\xi}_2$:

$$\nabla^2\boldsymbol{\xi}_1 = 0, \tag{16}$$

$$\nabla\cdot\boldsymbol{\xi}_1 = 0, \tag{17}$$

$$\begin{aligned}\rho\frac{\partial^2}{\partial t^2}(\nabla^2\xi_{2x}) = \frac{4\mu_0 H_p k}{\delta^2}\exp\Big\{\Big(\alpha+\frac{1}{\delta}\Big)x\Big\}\cos kz\cos\omega t \\ \times\Big[h_{f2}\cos\Big(\beta-\frac{1}{\delta}\Big)x-h_{f1}\sin\Big(\beta-\frac{1}{\delta}\Big)x\Big],\end{aligned} \tag{18}$$

$$\begin{aligned}\rho\frac{\partial^2}{\partial t^2}(\nabla^2\xi_{2z}) = a\frac{4\mu_0 H_p}{\delta^2}\exp\Big\{\Big(\alpha+\frac{1}{\delta}\Big)x\Big\}\sin kz\cos\omega t \\ \times\Big[\Big\{\Big(\alpha+\frac{1}{\delta}\Big)h_{f2}-\Big(\beta-\frac{1}{\delta}\Big)h_{f1}\Big\}\cos\Big(\beta-\frac{1}{\delta}\Big)x \\ -\Big\{\Big(\alpha+\frac{1}{\delta}\Big)h_{f1}+\Big(\beta-\frac{1}{\delta}\Big)h_{f2}\Big\}\sin\Big(\beta-\frac{1}{\delta}\Big)x\Big],\end{aligned} \tag{19}$$

where $$\nabla^2 = \Big(\frac{\partial^2}{\partial x^2}+\frac{\partial^2}{\partial z^2}\Big).$$

A suitable solution for $\boldsymbol{\xi}_1$, which is periodic in z and which obeys the condition that

its x-component is zero at the bottom of the fluid, $x = -a$, is

$$\xi_{1x} = X \frac{\sinh k(x+a)}{\sinh ka} \cos(kz) \cos(\omega t), \tag{20}$$

$$\xi_{1z} = -X \frac{\cosh k(x+a)}{\sinh ka} \sin(kz) \cos(\omega t), \tag{21}$$

where X is a coefficient to be determined. This motion for $\boldsymbol{\xi}_1$ is simply the motion of an ordinary linearized hydrodynamic surface wave. A solution for $\boldsymbol{\xi}_2$ is

$$\xi_{2x} = \exp\{(\alpha + 1/\delta)x\} \cos(kz) \cos(\omega t) \left[A \cos\left(\beta - \frac{1}{\delta}\right)x + B \sin\left(\beta - \frac{1}{\delta}\right)x\right], \tag{22}$$

$$\xi_{2z} = \exp\{(\alpha + 1/\delta)x\} \sin(kz) \cos(\omega t) \left[C \cos\left(\beta - \frac{1}{\delta}\right)x + D \sin\left(\beta - \frac{1}{\delta}\right)x\right], \tag{23}$$

where

$$A = \frac{\mu_0 H_p k}{\omega^2 \rho \delta(\alpha^2 + \beta^2)} [(\alpha - \beta) h_{f1} - (\alpha + \beta) h_{f2}], \tag{24}$$

$$B = \frac{\mu_0 H_p k}{\omega^2 \rho \delta(\alpha^2 + \beta^2)} [(\alpha + \beta) h_{f1} + (\alpha - \beta) h_{f2}], \tag{25}$$

$$C = \frac{\mu_0 H_p}{\omega^2 \rho \delta(\alpha^2 + \beta^2)} \left[\left(-\alpha^2 - \beta^2 + \frac{2\beta}{\delta}\right) h_{f1} + \left(\alpha^2 + \beta^2 + \frac{2\alpha}{\delta}\right) h_{f2}\right], \tag{26}$$

$$D = \frac{-\mu_0 H_p}{\omega^2 \rho \delta(\alpha^2 + \beta^2)} \left[\left(\alpha^2 + \beta^2 + \frac{2\alpha}{\delta}\right) h_{f1} + \left(\alpha^2 + \beta^2 - \frac{2\beta}{\delta}\right) h_{f2}\right]. \tag{27}$$

Because of the rapid decay of $\boldsymbol{\xi}_2$ in the x-direction, the effect of the bottom plate on this component of the motion is negligible, if a/δ is greater than 2. Therefore, the effects of the bottom have not been included in solving for $\boldsymbol{\xi}_2$.

Since the displacement of the free surface was assumed to be

$$\xi_0 \cos(kz) \cos(\omega t),$$

the coefficient X in (20) and (21) must be

$$X = \xi_0 - A. \tag{28}$$

Thus, by (13) and (20) to (28), the complete motion of the fluid has been determined. The principal characteristics of the motion become more apparent if α, β, h_{f1} and h_{f2} in the expressions for the coefficients A, B, C and D are replaced by their expansions in powers of δk, given as equations (A 8) to (A 11) of the appendix. For $\delta k \ll 1$, the dominant terms of the fluid displacement are

$$\xi_x = \xi_0 \cos(kz) \cos(\omega t) \left[\left\{1 + \frac{\mu_0 H_p^2 k^2}{4\omega^2 \rho} \delta k \coth(kb)\right\} \frac{\sinh k(x+a)}{\sinh(ka)} - \left\{\frac{\mu_0 H_p^2 k^2}{4\omega^2 \rho} \delta k \coth(kb)\right\} e^{2x/\delta}\right], \tag{29}$$

$$\xi_z = \xi_0 \sin(kz) \cos(\omega t) \left[-\left\{1 + \frac{\mu_0 H_p^2 k^2}{4\omega^2 \rho} \delta k \coth(kb)\right\} \frac{\cosh k(x+a)}{\sinh(ka)} + \left\{\frac{\mu_0 H_p^2 k^2}{2\omega^2 \rho} \coth(kb)\right\} e^{2x/\delta}\right]. \tag{30}$$

The magnetic field directly affects only the fluid within a shallow layer about one-half of a skin depth thick at the free surface. As seen from (30), the fluid in this layer is driven parallel to the fluid interface by the magnetic field in a direction which tends to be opposite to the z-component of the displacement of the main bulk of the fluid. This tangentially displaced fluid accumulates every half wavelength and reduces the displacement of the interface relative to the surface displacement which would correspond to the motion of the main bulk of the fluid.

Using the expressions for the fluid displacement, $\boldsymbol{\xi}$, as given by (13) and (20) to (28), and using (12) for $\nabla \cdot \mathbf{M}$ the fluid pressure p is obtained by integrating (2), the fluid equation of motion. The final result is:

$$\begin{aligned} p = \cos(kz)\cos(\omega t)\Bigg[&\frac{\omega^2\rho}{k}\frac{\cosh k(x+a)}{\sinh ka} \\ &\times\left\{\xi_0 - \frac{\mu_0 H_p k}{\omega^2\rho\delta}\frac{(\alpha-\beta)h_{f1}-(\alpha+\beta)h_{f2}}{\alpha^2+\beta^2}\right\} \\ &-\frac{2\mu_0 H_p}{k\delta^2(\alpha^2+\beta^2)}\exp\{(\alpha+1/\delta)x\}\Big\{(\beta h_{f1}+\alpha h_{f1})\cos\left(\beta-\frac{1}{\delta}\right)x \\ &+(\beta h_{f2}-\alpha h_{f1})\sin\{\beta-(1/\delta)\}x\Big\}\Bigg]. \end{aligned} \tag{31}$$

It is by means of the steep pressure gradients appearing in the second half of this expression that the force of electromagnetic origin is coupled to the fluid.

Dispersion relation

The wave dispersion relation is obtained by writing a stress balance equation at the surface of the fluid. If the stresses are linearized and evaluated at $x = 0$, instead of at the actual perturbed interface, the normal stresses to be balanced are: (i) the fluid pressure, p, given by (31) and evaluated at $x = 0$, which acts upward; (ii) the surface tension stress, $T(\partial^2\xi_x/\partial z^2)|_{x=0}$, which also acts upward; (iii) the gravitational stress, $\rho g\xi_x|_{x=0}$, due to the fluid which is raised or depressed from the equilibrium surface, and which acts downward when g is taken as a positive number; and (iv) a stress due to the unperturbed component of the magnetic field which acts on the perturbed surface. This last stress, which acts upward, is given by

$$\begin{aligned} p_{\text{mag}} &= \int_{x=0}^{\xi_0\cos(kz)\cos(\omega t)} (\nabla\cdot\mathbf{M})_x dx \\ &= -\int_{x=0}^{\xi_0\cos(kz)\cos(\omega t)} \frac{\mu_0 H_{0z}^2}{2\delta} dx \end{aligned} \tag{32}$$

when linearized. Dropping the high frequency terms, performing the integration, and expanding the exponential appearing in H_{0z}^2 to first order in ξ_0/δ, this stress is seen to be

$$p_{\text{mag}} = -\frac{\mu_0 H_p^2 \xi_0}{2\delta}\cos(kz)\cos(\omega t). \tag{33}$$

There are no unbalanced tangential stresses at $x = 0$ in this linearized analysis, since fluid viscosity has been neglected and since the tangential magnetic forces

are already balanced by the ξ_2 motion. The stress balance then leads to

$$\frac{\omega^2\rho}{k}\coth(ka)\left[\xi_0-\frac{\mu_0 H_p k}{\omega^2\rho\delta}\frac{(\alpha-\beta)h_{f1}-(\alpha+\beta)h_{f2}}{\alpha^2+\beta^2}\right]$$
$$-\frac{2\mu_0 H_p}{k\delta^2}\frac{\beta h_{f1}+\alpha h_{f2}}{\alpha^2+\beta^2}-Tk^2\xi_0=\rho g\xi_0+\frac{\mu_0 H_p^2\xi_0}{2\delta}, \qquad (34)$$

which is the wave dispersion relation. The dispersion relation is obtained in a form more suited for comparison with the experimental results if α, β, h_{f1} and h_{f2} are written as power series expansions in terms of δk, as given by (A 8) to (A 11) of the appendix. Then, for $\delta k \ll 1$, the dispersion relation becomes

$$\omega^2\rho\coth(ka)=Tk^3+\rho gk$$
$$+\frac{\mu_0 H_p^2 k^2}{2}\left[\coth(kb)+\frac{\delta k}{2}\{1-\coth^2(kb)-\coth(ka)\coth(kb)\}\right], \qquad (35)$$

correct to the first power in δk. The assumptions made in the derivation of this equation further restrict its application to cases where $\delta \ll a$.

Comparison with experiment

The experimental observations of the variation of the frequency shift slope with skin depth, presented in figure 4 *a*, *b*, *c*, are now compared with the theory developed above.

The data for the third mode are contained in figure 4 *a*. Assuming that the wavelength of this mode is 4·0 cm, the parameter δk is calculated to be 0·63 at 6 kc/s and 0·14 at 130 kc/s. The depth of the fluid, a, was estimated to be about 0·6 cm in this experimental run, and hence the distance to the top plate of the resonator assembly, b, is 4·2 cm. The values predicted from (35) for the slopes of the frequency squared versus H_0^2 curves are:

$$\frac{\Delta f^2}{\Delta H_0^2}\approx\frac{\mu_0 k^2}{4\pi^2\rho\coth ka}[0{\cdot}57] \qquad (36)$$

at 6 kc/s, and

$$\frac{\Delta f^2}{\Delta H_0^2}\approx\frac{\mu_0 k^2}{4\pi^2\rho\coth ka}[0{\cdot}90] \qquad (37)$$

at 130 kc/s. The ratio of these two predicted slopes is 0·57/0·90 = 0·63. However, the curves of figure 4 *a* show slopes of $5{\cdot}2\times10^{-3}\,\mathrm{c^2\,cm^2/A^2\,s^2}$ and $2{\cdot}0\times10^{-3}\,\mathrm{c^2\,cm^2/A^2\,s^2}$ at the two frequencies respectively. The ratio of these two experimental slopes is 0·38, which is smaller than the predicted ratio. Direct calculation from (34), using (A 6) and (A 7), gives predicted values only slightly different from those given in (36) and (37), which were calculated from the equation for the small δk limit.

Assuming that the wavelength for the first mode is 12·0 cm, the parameter δk is calculated to be 0·21 at 6 kc/s and 0·046 at 130 kc/s. The depth of the fluid a, was estimated to be about 0·7 cm in these particular experimental runs, and hence the distance b is 4·1 cm. The values predicted from (35) for the slopes of the frequency squared *vs.* H_0^2 curves are:

$$\frac{\Delta f^2}{\Delta H_0^2}\approx\frac{\mu_0 k^2}{4\pi^2\rho\coth ka}[0{\cdot}70] \qquad (38)$$

at 6 kc/s, and $$\frac{\Delta f^2}{\Delta H_0^2} \approx \frac{\mu_0 k^2}{4\pi^2 \rho \coth ka}\,[0{\cdot}96] \tag{39}$$

at 130 kc/s. The ratio of these two predicted slopes is $0{\cdot}70/0{\cdot}96 = 0{\cdot}73$. The curves of figure 4*b* show slopes of $9 \times 10^{-4}\,c^2\,cm^2/A^2s^2$ at 6 kc/s, and $10 \times 10^{-4}\,c^2\,cm^2/A^2s^2$ at 130 kc/s. The ratio of these two experimental slopes is 0·90, which is larger than the predicted ratio. On the other hand, the curves of figure 4*c* for the same experiment run 16 days later show slopes of $8{\cdot}6 \times 10^{-4}\,c^2\,cm^2/A^2s^2$ at 6 kc/s, and $12 \times 10^{-4}\,c^2\,cm^2/A^2s^2$ at 130 kc/s. The ratio of these two experimental slopes is 0·72, which is essentially the same as the predicted ratio. A comparison of the two results for the first mode shows that there is a considerable lack of reproducibility in the experiment. However, the experiments always yield a decrease in the frequency shift slope whose magnitude is within about a factor of two of the theoretically predicted decrease. Therefore, although a completely reproducible experiment was not obtained, the analysis is capable of predicting the behaviour of the waves to a useful level of accuracy.

4. Conclusion

The experiments described in §2 demonstrate one case where it is possible to create a high magnetic Reynolds number hydrodynamic system in the laboratory by using high frequency magnetic fields. A related hydrodynamic phenomenon which can be studied by using liquid metals in alternating magnetic fields is the stabilization of the Rayleigh–Taylor instability by a magnetic field parallel to the free surface (Chandrasekhar 1961). Since it is a Rayleigh–Taylor instability which limits the amount of metal that can be successfully levitated by a magnetic field, this is a problem of practical significance (Okress *et al.* 1952; Peifer 1965; Zhezherin 1959; Weisberg 1959). It is impossible to stabilize completely a fluid interface against the Rayleigh–Taylor instability with a d.c. magnetic field, even if the fluid is perfectly conducting, because of the directionality of the magnetic field. However, with a.c. magnetic fields, either a rotating magnetic field can be applied or two magnetic fields at two different frequencies can be applied perpendicular to one another, so that the magnetic field is non-directional in the time-average sense. Both these possibilities have been suggested by Zhezherin.

Another approach to suppression of the Rayleigh–Taylor instability on a fluid interface is to use continuum feedback to the interface through the magnetic fields, as suggested by Melcher (1966). Again, alternating magnetic fields must be used in an experimental study of such a system, since this is the most practical way to obtain a high magnetic Reynolds number.

The principal condition that must be met in all such experimental studies is that the skin depth must be smaller than about $\frac{1}{10}$ of the shortest wavelength to be stabilized.

Other hydromagnetic systems which can be studied by using liquid metals in alternating magnetic fields are the linear pinch and the theta pinch. Not only should the basic pinch instabilities be observable, but it should be possible to demonstrate hydromagnetic minimum-B stabilization, a topic of current interest in plasma confinement. Furthermore, by using several a.c. magnetic fields at

different frequencies, it is possible to construct novel time-average minimum-B systems.

This article is based on a doctoral thesis, written while the author was studying on a National Science Foundation Cooperative Graduate Fellowship. The author wishes to acknowledge the help of Prof. J. R. Melcher, his thesis supervisor, and Profs. H. A. Haus, W. D. Jackson and J. G. Siambis, who were on his thesis committee. Prof. E. S. Pierson and Mr R. Porter helped greatly by sharing their experience in the handling of NaK. The experimental work was supported in part by NASA Grant NsG-368.

Appendix

The magnetic field in the vacuum region above the fluid must satisfy Laplace's equation. Taking account of the effect of the highly conducting plate at $x = b$, a solution for $\mathbf{h}_v$, the perturbation to the uniform applied field that is sufficiently general to match conditions at the interface is:

$$h_{vx} = \frac{\sinh k(b-x)}{\sinh kb} \sin(kz) \sum_{\pm} [h_{v1} \cos \omega_{\pm} t + h_{v2} \sin \omega_{\pm} t], \tag{A 1}$$

$$h_{vz} = -\frac{\cosh k(b-x)}{\sinh kb} \cos(kz) \sum_{\pm} [h_{v1} \cos \omega_{\pm} t + h_{v2} \sin \omega_{\pm} t]. \tag{A 2}$$

Since there cannot be a surface current in a finitely conducting material, the magnetic field must be continuous across the fluid-vacuum interface,

$$\xi = \xi_0 \cos(kz) \cos(\omega t).$$

The condition for continuity of the z-component of the field is

$$H_p \cos(\omega_0 t) + h_{vz}|_{x=\xi} = h_{fz}|_{x=\xi} + H_p \exp -\{(\xi_0/\delta) \cos(kz) \cos(\omega t)\} \cos[\omega_0 t + (\xi_0/\delta) \cos(kz) \cos(\omega t)]. \tag{A 3}$$

If the perturbation to the fluid is so small that $\xi_0/\delta \ll 1$, then (A 3) can be linearized, giving

$$h_{vz}|_{x=0} = h_{fz}|_{x=0} + (\xi_0 H_p/2\delta) \sum_{\pm} [\cos \omega_{\pm} t - \sin \omega_{\pm} t] \cos(kz). \tag{A 4}$$

The linearized condition for continuity of the x-component of the field can be written down directly as

$$h_{vx}|_{x=0} = h_{fx}|_{x=0}. \tag{A 5}$$

Expressions for $\mathbf{h}_f$ from (8) and (9), and for $\mathbf{h}_v$ from (A 1) and (A 2) are then substituted into the continuity conditions, (A 4) and (A 5), where equating terms with like time dependence gives four equations in the unknown coefficients h_{f1}, h_{f2}, h_{v1} and h_{v2}. Solving this set of equations yields:

$$h_{f1} = -\frac{k\xi_0 H_p}{2\delta} \frac{\alpha + \beta + k \coth kb}{\alpha^2 + \beta^2 + 2\alpha k \coth kb + k^2 \coth^2 kb} \tag{A 6}$$

$$h_{f2} = \frac{k\xi_0 H_p}{2\delta} \frac{\alpha - \beta + k \coth kb}{\alpha^2 + \beta^2 + 2ak \coth kb + k^2 \coth^2 kb}. \tag{A 7}$$

There is no need to solve for h_{v1} and h_{v2}.

When $\delta k \ll 1$, power series expansions of α, β, h_{f1} and h_{f2} are more convenient than the exact expressions. These series expansions are:

$$\alpha = \frac{1}{\delta} + \tfrac{1}{4}\delta k^2, \tag{A 8}$$

$$\beta = \frac{1}{\delta} - \tfrac{1}{4}\delta k^2, \tag{A 9}$$

correct to third-order terms in δk (which happen to be zero) and

$$h_{f1} = -\frac{k\xi_0 H_p}{2}[1 - \tfrac{1}{2}\delta k \coth(kb)], \tag{A 10}$$

$$h_{f2} = \frac{k\xi_0 H_p}{2}\left[\tfrac{1}{2}\delta k \coth(kb) + \delta^2 k^2 \left(\frac{1}{4} - \frac{\coth^2 kb)}{2}\right)\right], \tag{A 11}$$

correct to second order in δk.

REFERENCES

CHANDRASEKHAR, S. 1961 *Hydrodynamic and Hydromagnetic Stability*. Oxford University Press.

COLGATE, S. A., FURTH, H. P. & HALLIDAY, F. O. 1960 *Rev. Mod. Phys.* **32**, 744.

DEVITT, E. B. & MELCHER, J. R. 1965 *Phys. Fluids*, **8**, 1193.

KRUSKAL, M. D. & SCHWARZSCHILD, M. 1954 *Proc. Roy. Soc.* A **223**, 348.

MELCHER, J. R. 1963 *Field-Coupled Surface Waves*. Cambridge, Mass: M.I.T. Press.

MELCHER, J. R. 1966 *Phys. Fluids*, **9**, 1973.

OKRESS, E. C., WROUGHTON, D. M., COMENTZ, G., BRACE, P. H. & KELLEY, J. G. R. 1952 *J. Appl. Phys.* **23**, 545.

OSOVETS, S. M. 1963 *Atomnaya Energia*, **15**, 283 in Russian. English transl. 1964 in *Plasma Phys. Accelerators-Thermonuclear Res.* **6**, 421.

PEIFER, W. A. 1965 *J. of Metals*, **17**, 487.

ROOK, C. W. 1964 Sc.D. Thesis, Dept. of Electrical Engineering, Massachusetts Institute of Technology, Cambridge, Mass.

WEISBERG, L. R. 1959 *Rev. Sci., Instrum.* **30**, 135.

ZHEZHERIN, R. P. 1959 In the collection *Voprosi Magnitnoy Gidrodinamiki i Dinamiki Plasmi*, Akad. Nauk Latv. SSR, Riga, Latvia, SSR, 279, in Russian.